LATTICE BOLTZMANN SIMULATION OF HEAT TRANSFER ENHANCEMENT DURING MELTING BY USING NANOPARTICLES[*]

A. A. RABIENATAJ DARZI , M. FARHADI[**] AND M. JOURABIAN

Faculty of Mechanical Engineering, Babol University of Technology, Babol, Islamic Republic of Iran, P.O. Box 484
Email: mfarhadi@nit.ac.ir

Abstract– This research paper provides a mathematical modeling of heat transfer enhancement during melting process in a square cavity through dispersion of nanoparticles. The enthalpy-based lattice Boltzmann method (LBM) with a combination of D2Q9 and D2Q5 lattice models is used to solve density, velocity and temperature fields. The nano-enhanced phase change material (NEPCM) is composed of a dilute suspension of copper particles in water (ice) and is melted from the left. Also, in this study the sub-cooling case is neglected. Conduction heat transfer has been taken into account in the solid phase as well as natural convection in the liquid phase. Numerical simulations are performed for various volume fractions of nanoparticles and Rayleigh numbers ranging from 10^4 to 10^6. The validation of results is carried out by comparing the present results of natural convection and convection-dominated melting in a square cavity with those of existing earlier numerical studies. Predicated results illustrate that by suspending the nanoparticles in the fluid the thermal conductivity of NEPCM is increased in comparison with PCM. Also, by enhancing thermal conductivity and decreasing latent heat of fusion higher rates of heat release can be obtained.

Keywords– Nanoparticles, lattice boltzmann method, phase change, melting, enthalpy method

1. INTRODUCTION

Solid-liquid phase change phenomena, either melting or solidification, occur often in many industrial processes as well as in nature. They especially appear in applications such as latent heat thermal energy storage systems (LHTESS), purification, removal of heat from electronic components, molding, growth of crystals, laser manufacturing, drilling and so forth.

Phase change materials (PCMs) are ideal products for the purpose of thermal energy storage whereby thermal energy can be stored at a constant temperature during phase change. The PCMs that have been subdivided by many authors into organic, non-organic and eutectics compounds experience reversible phase transformations. However, it must be mentioned that the main unacceptable property of most PCMs, as examined by many researchers is their low thermal conductivity that prevents high rates of energy charging and discharging. So it is highly recommended to enhance thermal conductivity of PCM with various techniques such as fins, insertion of a metal matrix, metal honeycombs, using dispersing high conductivity particles into the PCM, etc.

In recent years, nanofluids have attracted greater interest in various engineering applications because of the remarkable increase in effective thermal conductivity of base fluid [1]. Masuda et al. [2] reported on improved thermal conductivity of dispersed ultra-fine (nanosize) particles in liquids. Choi [3] was the first to coin the term "nanofluids" for this new class of fluids with superior thermal properties. Khanafer et al. [4] investigated the heat transfer enhancement in a two-dimensional enclosure using nanofluids for a range

of Grashof numbers and volume fractions. Ranjbar et al. [5] studied numerically the effect of utilizing nanoparticle on the solidification phase front inside a rectangular container. Their findings showed that with an increase in the nanoparticles volume fraction the nanofluid heat transfer augments. Also, their results showed that conduction is the main mode of heat transfer in both phases. The effect of nanoparticle dispersion in a concentric annulus was investigated by Sebti et al. [6]. Their study showed that the suspended nanoparticles decrease the solidification time and it is possible to improve the traditional energy storage systems if the amount of suspended nanoparticles within the PCMs is properly chosen.

Recently LBMs have become a powerful technique for the computational modeling of a wide variety of complex fluid flow problems including single and multiphase flow in complex geometries [7-14]. Nemati et al. [15] found the effect of various nanofluids on mixed convection flows using an LB model that is the same as that used in Refs [16-18]. Yang and Lai [19] examined numerically the flow and heat transfer characteristics of alumina-water in a microchannel using LBM. This paper proved that LBM is a capable method for predictions of flow and heat transfer in a microchannel. These authors also made a numerical effort to model natural convection in a square cavity that filled with Al_2O_3/water nanofluids using LBM [20]. The results indicated that with the use of nanofluid, the average Nusselt number becomes higher than that of using water for the same *Ra*. He et al. [21] developed an LB model by coupling density and temperature distribution functions to simulate natural convection using Al_2O_3-water nanofluids in a plain square cavity. They illustrated that the sensitivity of heat transfer and flow characteristics of Al_2O_3-water to viscosity is more than to thermal conductivity. The simulation of natural convection in tall enclosures using LBM was carried out by Kefayati et al. [22]. They explained that by increasing the aspect ratio of enclosure the impact of nanoparticles on nanofluid heat transfer enhances.

In the early studies of simulating melting, one-dimensional conduction was considered to be the major mechanism of heat transfer. Then this type of problem could be solved by analytical procedures. However, in more real applications natural convection induced in the liquid phase plays a key role on the shape and position of phase change front. So, the accurate prediction of solid-liquid phase change front becomes the main difficulty with the mathematical modeling of melting. In order to overcome this difficulty, complicated numerical methods have been proposed in the literature such as front tracking method [23]; level set method [24], adaptive grid method [25], and phase field method [26].

Investigation of natural convection melting in a cavity has been held experimentally [27-29], theoretically [30-31], and numerically [32-35].

Generally, the existing LBMs for solving solid-liquid phase transitions can be classified into two separate groups: first, enthalpy-based method [33, 36] and second, phase-field method based on the theory of Ginzburg-Landau [37-39]. By applying an enthalpy formula, the solid-liquid phase change problem becomes much simpler and has the following benefits:

1: it eliminates the need to satisfy boundary condition at the phase change front, 2: the temperature is evaluated at each node and then for the thermophysical properties can be determined, 3: it allows a mushy zone between the solid and liquid phases, 4: by using the temperature field, the position of solid-liquid phase change front can be discovered if recommended.

As mentioned above, by dispersing nanoparticles into PCM thermal conductivity of PCM will be improved. So, the aim of this research work is to numerically study melting with natural convection of NEPCM in a square cavity. A combination of D2Q9 and D2Q5 lattice models is used to solve both velocity and temperature fields. Besides, the enthalpy method is based on the modified version of Jiaung et al. [36] melting scheme. To validate our results, the liquid fraction and dimensionless temperature are solved based on the Huber et al. [40] work. The effect of various volume fractions of nanoparticles (0 to 0.03) on the melting rate is studied for Rayleigh numbers of $10^4, 10^5$ and 10^6. Also, Prandtl number and Stefan number are fixed to 6.2 and 1, respectively.

2. PHYSICAL MODEL AND GOVERNING EQUATIONS

The physical domain under examination is shown in Fig. 1. The PCM is primarily at the temperature of T_0. In the case of no subcooling, T_0 is equal to T_m. The right, top and bottom walls are adiabatic. The PCM begins to melt when the left wall is maintained at the temperature of T_1 ($T_1 > T_0$). The thermophysical properties of copper particles and water base were taken in Table 1. For the simulations the following assumptions are considered:

1: the flow in the liquid phase is a laminar, incompressible and Newtonian one, 2: the compression work done by the pressure and viscous heat dissipation are neglected, 3: the densities of solid and liquid phase are equal during melting, 4: the Boussinesq approximation is used for natural convection, 5: the process is considered as a conduction/convection controlled phase change problem, 6: the velocity of melted PCM is small enough.
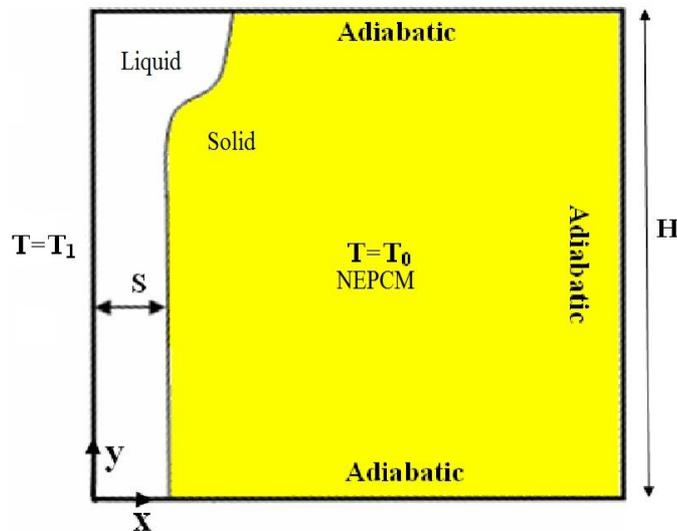

Fig. 1. Schematic of computational domain under investigation

Table 1. Thermo-physical properties of NEPCM

property	Copper nano-particles	Based fluid
ρ [kg m^{-3}]	8954	997.1
μ [Pa s]	-	8.9×10^{-4}
C_p [J kg^{-1} K^{-1}]	383	4179
k [w m^{-1} K^{-1}]	400	0.6
β	1.67×10^{-5}	2.1×10^{-4}
Ste	-	1

Therefore, the two dimensional of equations for natural convection with phase can be written as follows:

$$\frac{\partial u_i}{\partial x_i} = 0 \tag{1}$$

$$\frac{\partial u_i}{\partial t} + u_j \frac{\partial u_i}{\partial x_j} = \frac{1}{\rho_{nf}} \left(\mu_{eff} \nabla^2 u_i - \frac{\partial P}{\partial x_i} + (\rho\beta)_{nf} (T - T_{ref}) g_i \right) \tag{2}$$

$$\frac{\partial T}{\partial t} + u_i \frac{\partial T}{\partial x_i} = \frac{\partial}{\partial x_i}\left(\frac{k_{eff}}{(\rho C_p)_{nf}}\frac{\partial T}{\partial x_i}\right) - \frac{L_{nf}}{(\rho C_p)_{nf}}\frac{\partial F_l}{\partial t} \tag{3}$$

In these relations, u_i is the fluid velocity, ρ_{nf} is the NEPCM's density, μ_{eff} is the dynamics viscosity of NEPCM, P is the pressure, g is the gravitational acceleration, L_{nf} is the effective latent heat of phase change, k_{eff} is the effective thermal conductivity.

The density of the nanofluid is given by:

$$\rho_{nf} = (1-\phi)\rho_f + \phi\rho_s \tag{4}$$

Whereas the heat capacitance of the nanofluid and part of the Boussinesq term are:

$$(\rho c_p)_{nf} = (1-\phi)(\rho c_p)_f + \phi(\rho c_p)_s \tag{5}$$

$$(\rho\beta)_{nf} = (1-\phi)(\rho\beta)_f + \phi(\rho\beta)_s \tag{6}$$

with ϕ being the volume fraction of the solid particles and subscripts *f, nf* and *s* stand for base fluid, nanofluid and solid particle, respectively. The viscosity of the nanofluid containing a dilute suspension of small rigid spherical particles is given by:

$$\mu_{eff} = \frac{\mu_f}{(1-\phi)^{2.5}} \tag{7}$$

The effective thermal conductivity of nanofluid was given by Patel et al. [41] as follows:

$$k_{eff} = k_f + k_p\frac{A_p}{A_f} + c'k_p Pe\frac{A_p}{A_f} \tag{8}$$

Where c' is a constant and must be determined experimentally, A_p/A_f and *Pe* here are defined as:

$$\frac{A_p}{A_f} = \frac{d_p}{d_f}\frac{\phi}{(1-\phi)} \tag{9}$$

$$Pe = \frac{u_p d_p}{\alpha} \tag{10}$$

Where d_p is the diameter of solid particles and it is assumed to be equal to 100 nm, d_f is the molecular size of liquid that is taken as 2 Å for water. Also, u_p is the Brownian motion velocity of nanoparticle which is defined as:

$$u_p = \frac{2k_b T}{\pi\mu_f d_p^2} \tag{11}$$

Where k_b is the Boltzmann constant. The latent heat is evaluated using:

$$(\rho L)_{nf} = (1-\phi)(\rho L)_f \tag{12}$$

It is clear that Eqs. (11) and (12) were employed in the liquid region of NEPCM while other relations were applied in all regions of NEPCM.

3. LBM

a) LB equation for the velocity field

In the LBM, the particles are described by quantities f_i representing the particle density distributions. The main equation that needs to be solved is:

$$f_i(x+c_i\Delta t, t+\Delta t) - f_i(x,t) = \Omega_i \tag{13}$$

The collision term Ω_i on the right-hand side of Eq. (13) uses the so called Bhatangar-Gross-Krook (BGK) approximation [42]. This collision term will be substituted by the well-known classical single time relaxation approach:

$$\Omega_i = -\frac{f_i - f_i^{eq}}{\tau} + F_i \tag{14}$$

Where τ is the relaxation time depending on the fluid viscosity and f_i^{eq} is the local equilibrium distribution function that has properly prescribed dependence on the local physical properties. F_i is the external force in the direction of lattice velocity. In order to formulate buoyancy force in the natural convection problem, the Boussinesq approximation was applied and radiation heat transfer is insignificant, therefore the force term in the Eq. (14) needs to be computed as shown below in the vertical direction (y):

$$F_i = 3\omega_i \rho(x,t)\beta(T(x,t)-T_{ref})g.c_i \tag{15}$$

T_{ref} is the reference temperature. The LB equation for dynamical system is completed by choosing the equilibrium distribution [43]:

$$f_i^{eq} = \omega_i \rho\left[1+\frac{3}{c^2}c_i.u+\frac{9}{2c^4}(c_i.u)^2-\frac{3}{2c^2}u.u\right] \tag{16}$$

Where ω_i is the equilibrium distribution weight for direction of i.

$$\omega_i = \begin{cases} 4/9 & i=0 \\ 1/9 & i=1,2,3,4 \\ 1/36 & i=5,6,7,8 \end{cases} \tag{17}$$

c_i denotes the discrete velocity set for D2Q9 topology.

$$c_i = \begin{cases} (0,0) & i=0 \\ (\cos[(i-1)\pi/4],\sin[(i-1)\pi/4])c & i=1,2,3,4 \\ \sqrt{2}(\cos[(i-1)\pi/4],\sin[(i-1)\pi/4])c & i=5,6,7,8 \end{cases} \tag{18}$$

Where the streaming speed is defined as $c=\Delta x/\Delta t=1$. The density and velocity are obtained through moment summations in the velocity space:

$$\rho(x,t)=\sum_i f_i(x,t) \tag{19}$$

$$\rho u(x,t)=\sum_i c_i f_i(x,t) \tag{20}$$

The Chapman – Enskog expansion has already been used to obtain macroscopic equations such as for viscosity. The detailed derivation was given by Hou et al. [44] and will not be shown here. The viscosity is given by

$$v=(\tau_v-0.5)c_s^2\Delta t \tag{21}$$

c_s is the speed of sound and identified as $c_s^2=c^2/3$. The positivity of the viscosity requires $\tau_v>0.5$.

b) LB equation for the temperature field

In general, LB methods for a fluid flow involving heat transfer in a plain medium can be classified into four categories: multispeed (MS), entropic, hybrid and multi-distribution function (MDF) models. In the present study, the MDF approach [45-46] was chosen to simulate natural convection. The evolution equations for the temperature (g_i) in the fluid are also described by a BGK dynamic and are given as follows:

$$g_i(x+c_i\Delta t,t+\Delta t)-g_i(x,t)=-\frac{1}{\tau_T}(g_i(x,t)-g_i^{eq}(x,t)) \tag{22}$$

τ_T is the relaxation time for temperature field. The simplified equilibrium temperature distribution function is given by:

$$g_i^{eq}=T\,\omega_i^T\,[1+\frac{1}{c_s^2}(v_i.u)] \tag{23}$$

Where v_i and ω_i^T are the associated lattice velocities and weights. For the evolution of g_i, a D2Q5 lattice is chosen. In this topology, the velocities v_i are:

$$v_i=\begin{cases} (0,0) & i=0 \\ (\cos[(i-1)\pi/2],\sin[(i-1)\pi/2]) & i=1,2,3,4 \end{cases} \tag{24}$$

The associated weights, ω_i^T are $\omega_0^T=\frac{1}{3},\omega_i^T=\frac{1}{6}$ for i = 1,2,3,4. The macroscopic temperature is calculated from:

$$T=\sum_{i=0}^4 g_i \tag{25}$$

Through the Chapman-Enskog expansion, the energy equation can be exactly recovered from LB equation. The thermal diffusivity is associated with non-dimensional thermal relaxation time by Eq. (26):

$$\alpha=\frac{c^2}{6}\left(2\tau_T-\Delta t\right) \tag{26}$$

By adjusting τ and τ_T, the MDF technique provides the feasibility to change *Pr*.

c) Phase change treatment with LBM

To solve phase change problem, a slightly modified version of Jiaung et al. [36] melting scheme is

used. They used enthalpy method to find both temperature and liquid fraction. In the enthalpy technique, the phase change front is not explicitly tracked. Instead, an amount named the liquid fraction, which shows the fraction of the cell volume that is in liquidized form, is related to each cell. The liquid fraction is calculated at each iteration based on the value of enthalpy. Hence, the phase change front conditions are automatically attained. It also creates a mushy zone in which the liquid fraction varies from 0 to 1. This zone prevents some discontinuities that may lead to some numerical instabilities.

The local enthalpy at the time step *n* and iteration *k* is evaluated according to Eq. (27) as:

$$En^{n,k} = c_p\, T^{n,k} + L_f\, f_l^{n,k-1} \tag{27}$$

The liquid fractions at the current iteration level are then updated:

$$f_l^{n,k} = \begin{cases} 0 & En^{n,k} < En_s = c_p\, T_m & solid\ zone \\ \dfrac{En^{n,k} - En_s}{En_l - En_s} & En_s \le En^{n,k} \le En_s + L_f & mushy\ zone \\ 1 & En^{n,k} > En_s + L_f & liquid\ zone \end{cases} \tag{28}$$

where T_m is the melting temperature. Afterwards the temperature distribution functions are acquired by

$$g_i^{n,k}(x+c_i\Delta t, t+\Delta t) = g_i(x,t) - \frac{1}{\tau_T}(g_i(x,t) - g_i^{eq}(x,t)) - \omega_i \frac{L_f}{c_p}(f_l^{n,k} - f_l^{n-1})) \tag{29}$$

d) Nano fluid treatment with LBM

The dimensionless relaxation time for velocity and thermal fields which are evaluated by the nanofluid properties are as follows:

$$\tau_v = \frac{3}{2}\frac{\nu_{nf\,(lbm)}}{c^2\Delta t} + 0.5 = \frac{3}{2}\frac{\mu_{nf\,(lbm)}}{\rho_{nf\,(lbm)}c^2\Delta t} + 0.5 \tag{30}$$

$$\tau_T = \frac{3}{2}\frac{\alpha_{nf\,(lbm)}}{c^2\Delta t} + 0.5 = \frac{3}{2}\frac{k_{nf\,(lbm)}}{(\rho c_p)_{nf\,(lbm)}c^2\Delta t} + 0.5 \tag{31}$$

That *lbm* subscript determines the lattice scale. This technique is the same with Das et al. [47] and Wang et al. [48] in simulation of variable thermal conductivity in LB.

Also, the parameters of c_p, β and L_f should be replaced with $(c_p)_{nf}$, β_{nf} and L_{nf} into related equations in the previous section.

e) Boundary conditions

The commonly used type of boundary condition in LBM is the bounce-back boundary scheme. This scheme is usually used to obtain no-slip velocity conditions. By the so-called bounce-back scheme, it means that when a particle distribution streams to a stationary wall node, the particle distribution reflects back to the original node fluid, but with the direction rotated by π radians. For the left wall, the entering distribution functions at *i=3,6* and *7* directions are known because they stream from the nodes inside the flow field but the leaving distribution functions at *i=1,5* and *8* directions are unknown, which can be determined from the known distribution functions as follows:

$$f_{\bar{i}}^{out} = f_i^{in} \tag{32}$$

The temperature at the left wall is kept at $T_1 = 1$(i.e. prescribed temperature). So, a Dirichlet boundary condition can be imposed on this wall. To determine the only unknown distribution function for temperature, g_1, Eq. (25) is invoked as:

$$g_1 = 1 - (g_0 + g_2 + g_3 + g_4)$$

(33)

The remaining walls are adiabatic and require no heat conduction in the normal direction. For instance for right wall, the unknown distribution function, g_3 is determined by

$$g_{3,n} = g_{3,n-1}$$

(34)

Where n-1 show a lattice that is placed inside the cavity close to the boundary nodes.

f) Code validation

A first validation was made using the test case of natural convection in a square cavity [49]. The evaluation is fulfilled at three different Rayleigh numbers, 10^4, 10^5 and 10^6 and its results are shown in Table 2. As can be seen from Table 2, the accuracy of the present work in comparison with benchmark [49] is good.

Table 2. The validation of the current results in a square cavity

	$\dfrac{u_{max}H}{\alpha}$	$\dfrac{v_{max}H}{\alpha}$	Nu_m
Ra= 10^4			
Benchmark [49]	16.187	19.617	2.243
Present work	15.71	20.15	2.2394
Ra= 10^5			
Benchmark [49]	34.730	68.590	4.519
Present work	35.54	70.341	4.56
Ra= 10^6			
Benchmark [49]	64.630	219.36	8.800
Present work	58.43	223.1	8.95

Authors in previous work [15] performed an LB simulation of heat transfer enhancement in a lid driven cavity subjected to various side wall temperatures and filled with nanofluid. It was found that the straightforward implementation of effective thermal conductivity is the significant benefit of this method.

For melting process in a square cavity, the average Nusselt number on the left wall and the average melt front position as a function of dimensionless time were compared with the Huber et al. [40] work for $Ra=1.7\times10^5$, $Pr=1$ and $Ste=10$. As shown in Fig. 2, the comparison between the present study and the Huber et al. [40] work is quite satisfying because the maximum discrepancies in the results of average melting front position and average Nusselt number are 8 and 6 percent, respectively.

The height-averaged melting front location, S_{av}, and the average Nusselt number are computed as in Jany and Bejan [30]:

$$S_{av}(t) = \frac{1}{H} \int_0^H x_m dy \propto HRa^{1/4}\theta$$

(35)

$$Nu_m = \int_0^H \frac{\partial T^*}{\partial x^*}\left(x = 0, y\right)dy$$

(36)

Where x_m is the deformed melting front in the convection regime, x^* is equal to $\dfrac{x}{l}$ and T^* is $\dfrac{T - T_m}{T_1 - T_0}$.

Diverse grid sizes were chosen and checked to ensure the independency of result from the adopted grid size based on comparison of melting fraction. An arrangement of 200×200 grids was found sufficient for this study.
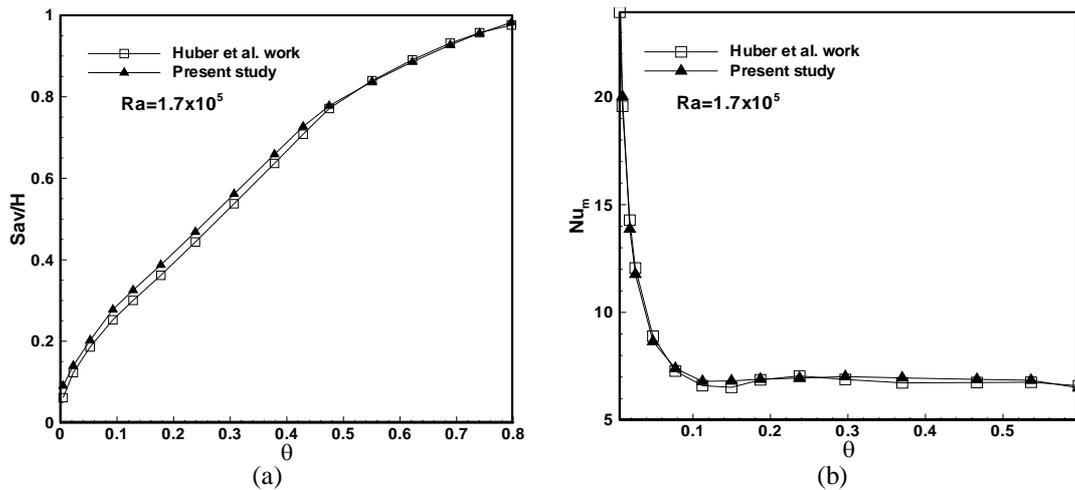

Fig. 2. Comparison of (a) average melting front position and (b) Nusselt number versus dimensionless time between present study and Huber et al's. [40] work for *Pr* =1 and *St*e =1

4. RESULTS AND DISCUSSIONS

The streamlines of a cavity with and without nanoparticles against dimensionless time are shown in Fig. 3 qualitatively. At the early stages of melting, $\theta = 0.0013$, no flow is monitored in the melted PCM, pure conduction heat transfer is the main mode of heat transfer, melting front moves vertically and it has a planar shape. At $\theta = 0.02$, a recirculation vortex is formed next to the left wall for both cases demonstrating the appearance of natural convection in the melted PCM. Afterwards the melted PCM floats up, causing the deformation of melting front. From Eq. (8) to Eq. (11) it can be inferred that by enhancing the temperature adjacent to the left wall, the effective thermal conductivity of nanofluid will be increased. So as time elapses, in the existence of nanoparticles the phase change front moves faster, particularly at the top section of the cavity in comparison with the pure fluid, ϕ=0. This is due to the augmentation of convection heat transfer and velocity of the molten PCM at this region.

As plotted in Fig. 4, temperature contours could be an indicator of liquid fractions where the dark blue color represents the un-melted PCM ($T=T_0$). For $\theta \geq 0.02$, it can be observed that melting rate in the top section of the cavity is higher than that of the bottom section. It is shown that the molten zone is very narrow in the left side of the bottom section where conduction heat transfer continues to dominate. At the end of melting, because of the extreme influence of natural convection in the top section, the phase change front becomes flatter almost like a horizontal line.
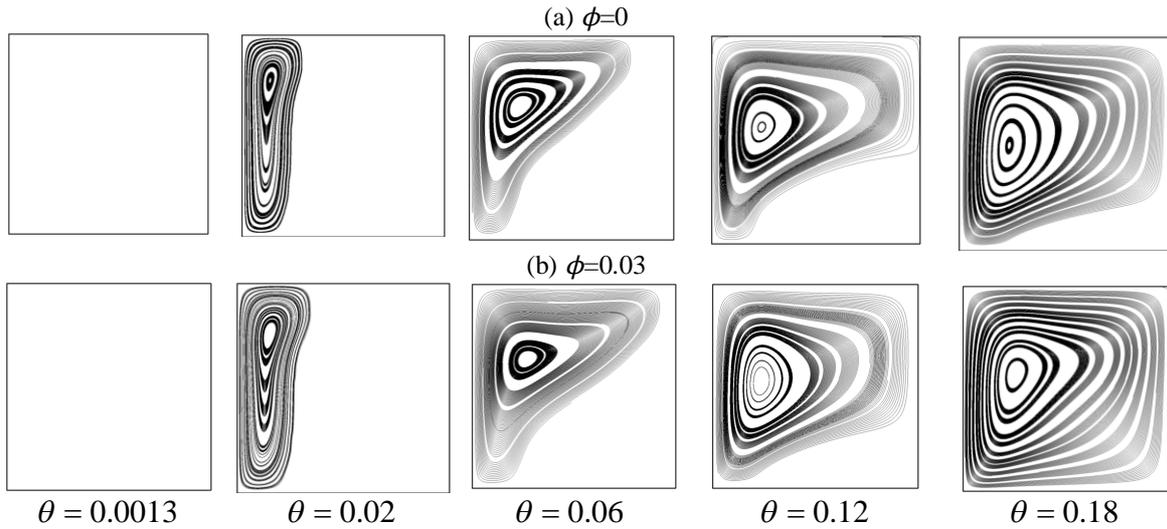
(a) ϕ=0

(b) ϕ=0.03

$\theta = 0.0013$ $\theta = 0.02$ $\theta = 0.06$ $\theta = 0.12$ $\theta = 0.18$

Fig. 3. Streamlines for a cavity with (a) ϕ=0 and (b) ϕ=0.03 at
different dimensionless times and $Ra =10^5$

T^* 0.00 0.05 0.11 0.16 0.21 0.26 0.32 0.37 0.42 0.47 0.53 0.58 0.63 0.68 0.74 0.79 0.84 0.89 0.95 1.00

(a) ϕ=0

(b) ϕ=0.03

$\theta = 0.0013$ $\theta = 0.02$ $\theta = 0.06$ $\theta = 0.12$ $\theta = 0.18$
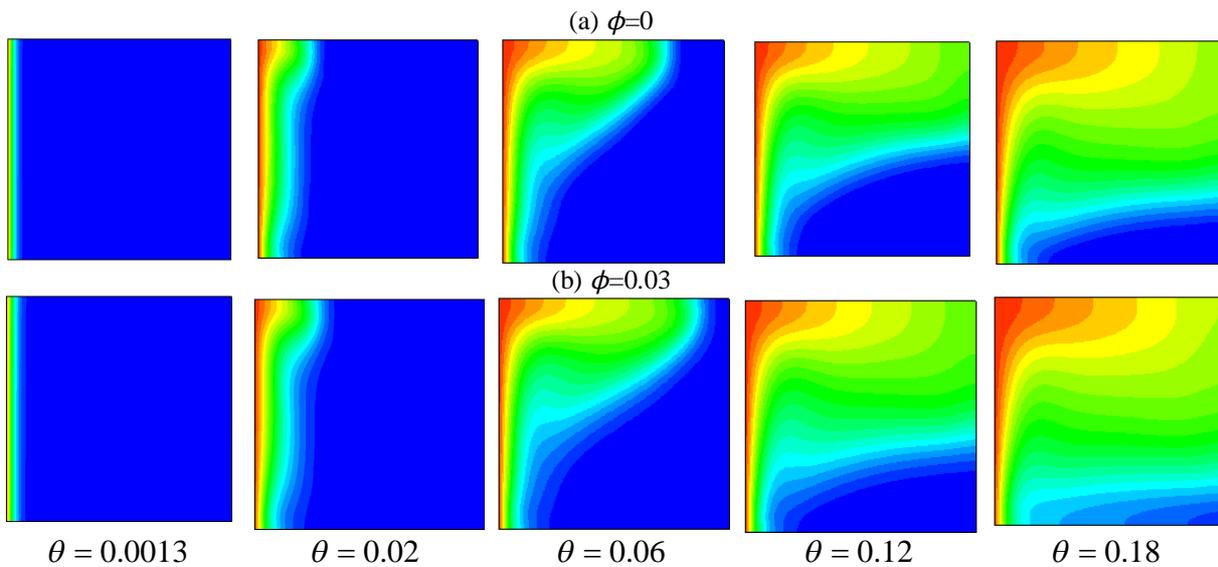
Fig. 4. Temperature contours for a cavity with (a) ϕ=0 and (b) ϕ=0.03 at
different dimensionless times and $Ra =10^5$

Figure 5 reveals the variations of average melting front versus dimensionless time for different Rayleigh numbers and solid concentrations. The slope of the graphs specifies the melting rate. At the beginning of melting, slopes are very sharp and melting rates are approximately equivalent in each case showing the domination of conduction heat transfer. It is demonstrated that the average melting front position is increased by enhancing solid concentrations in any Rayleigh number. Furthermore, with the increase of Rayleigh numbers the full melting of NEPCM occurs earlier than $Ra=10^4$. Unquestionably, that is because of the domination of natural convection, especially at the top section. It is obvious that by increasing the solid concentration from 0 to 0.03, full melting time declines approximately 38.3, 20.8 and 17.6 percent at Rayleigh numbers of 10^4, 10^5 and 10^6, respectively.
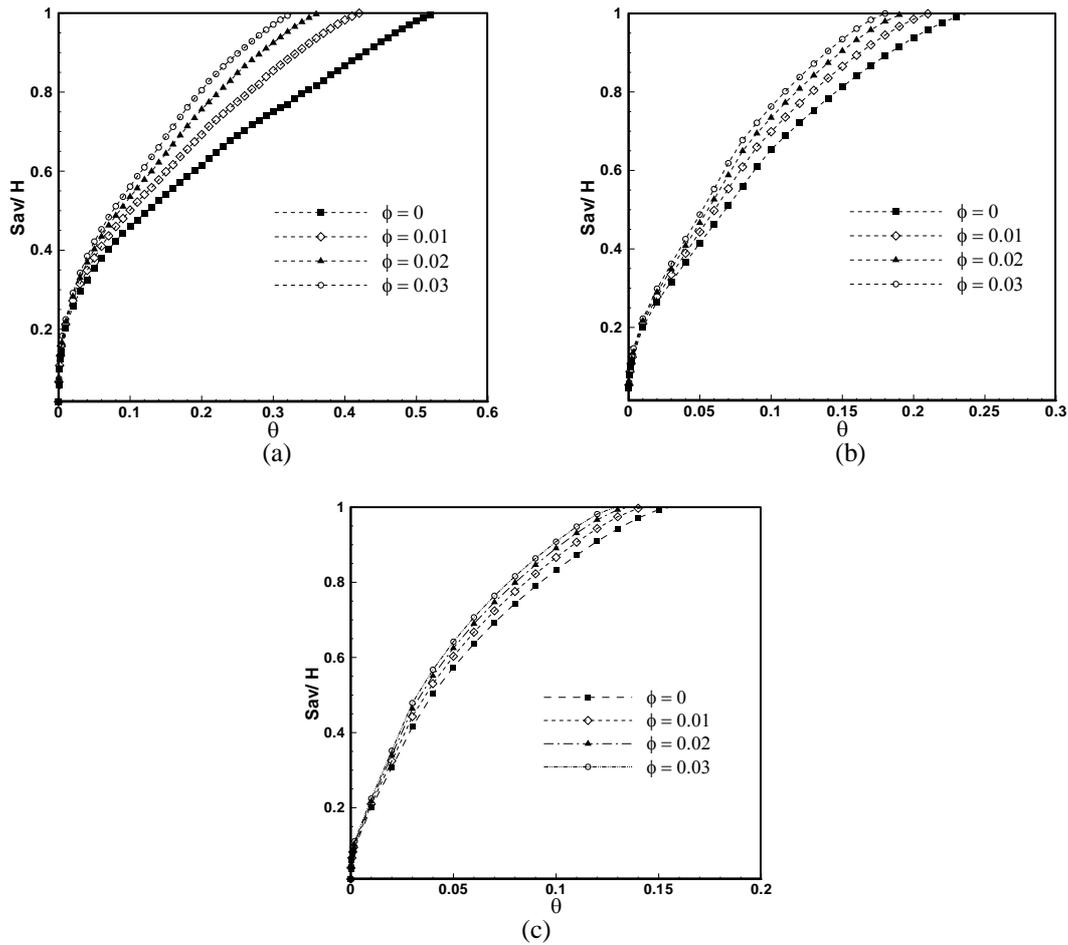
Fig. 5. Full melting time decline for various solid concentrations
(a) $Ra = 10^4$ (b) $Ra = 10^5$ (c) $Ra = 10^6$

Variations of dimensionless temperature versus dimensionless time at central point of cavity are illustrated in Fig. 6 for various solid concentrations. In this case Rayleigh number is fixed to 10^5. It can be observed that its temperature rises up faster through enhancement of solid concentrations. The fact is that by increasing the solid concentrations, melting rate enhances further so that melting front reaches faster to this point where the temperature starts to increase in a lesser time. The starting point of melting at this point takes place 14.3, 28.5 and 42.8 percent earlier when the solid concentration augmented from 0 to 0.03 by the step of 0.01, respectively.
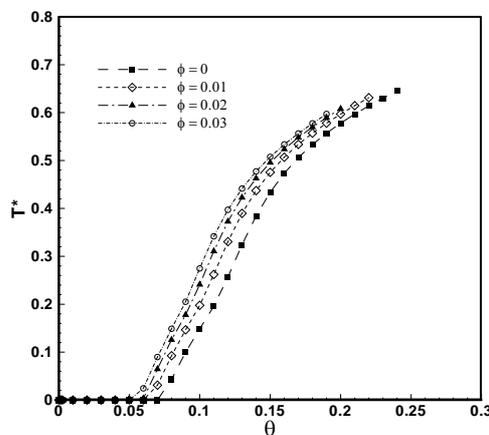

Fig. 6. Distribution of temperature at central point of cavity
for different solid concentrations at $Ra = 10^5$

Figure 7 depicts the effect of Rayleigh number on the temperature of central point for solid concentration of 0.01. As can be understood, altering the Rayleigh number has a noticeable effect on the temperature distribution. By increasing the Rayleigh number from 10^4 to 10^6, the beginning time of melting at the central point of the cavity decreases 55.5 percent and higher temperatures can be obtained.
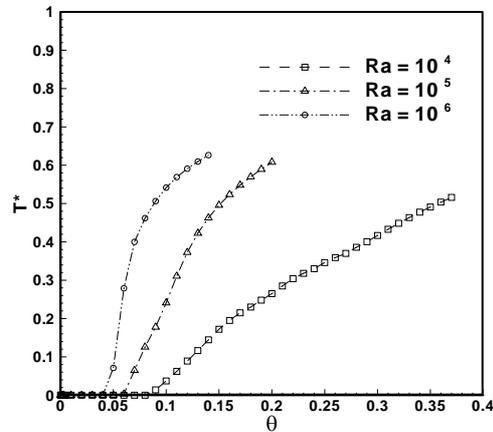

Fig. 7. Distribution of temperature at central point of cavity for
different Rayleigh numbers for $\phi = 0.02$

5. CONCLUSION

In the present research study, heat transfer enhancement of PCM through the dispersion of nanoparticles was investigated numerically by using enthalpy-based LBM. The lattice D2Q9 was implemented to determine the velocity and density fields, while the simplest lattice D2Q5 model was used for temperature field. A satisfactory validation between the present study and previous numerical results was carried out. Our findings are categorized as follows: (1): The obtained results confirm that conduction heat transfer plays a dominant role at the beginning of melting and as the process proceeds natural convection takes the key role. By adding nanoparticles into the PCM, the phase change front moves faster mainly at the top section in comparison with the pure fluid, ϕ=0. (2): It can be found that melting rate of PCM is noticeably intensified by adding copper nanoparticles, owing to the improvement of thermal conductivity and decline of the latent heat of fusion. (3): Also, it can be concluded that the NEPCM has great potential for TES purposes because the rate of heat release increases significantly.

NOMENCLATURE

c	Streaming speed[m]	*Subscripts*	
c_i	Discrete lattice velocity in direction i	f	based fluid
c_p	Heat capacity[Jkg^{-1}K^{-1}]	i	direction
c_s	Speed of sound in Lattice scale	nf	nanofluid
En	Total enthalpy[J]	ref	reference
En_s	Enthalpy of the solid phase[J]	s	nanoparticles
En_l	Enthalpy of the liquid phase[J]	*Superscripts*	
F_i	External force in direction of lattice velocity	n	time step
f_l	Liquid fraction	k	iteration
f_k^{eq}	Equilibrium distribution for velocity field	*Greek symbols*	

Fo	Fourier number $(\alpha t/l^2)$	β	Thermal expansion coefficient[K^{-1}]
g	Acceleration due to gravity force[ms^{-2}]	ρ	Density[kgm^{-3}]
g_k^{eq}	Equilibrium distribution for temperature field	τ	Lattice relaxation time
H	Height of cavity[m]	ϕ	Volume fraction of nanoparticles
l	Appropriate length scale[m]	θ	Dimensionless time $(\theta = Fo \times Ste)$
L_f	Latent heat of phase change[Jkg^{-1}]	α	Thermal diffusivity[m^{2}s^{-1}]
Nu_m	Average Nusselt number on the left wall	v	Kinetic viscosity[m^{2}s^{-1}]
Pr	Prandtl number (v/α)	Δx	Lattice cell size
Ra	Rayleigh number $(g\,\beta\,\Delta T\,l^3/\alpha v)$	Δt	Lattice time step size
Ste	Stefan number $(c_p\,\Delta T/L_f)$		
T_0	The initial temperature of PCM[K]		
T_1	The temperature of left wall[K]		
T_m	The melting temperature of PCM[K]		
T^*	Dimensionless temperature		
u	Velocity of the fluid[ms^{-1}]		
ω_i	Equilibrium distribution weight		
ω_i^T	The associated weight for temperature field		

REFERENCES

1. Xuan, Y. & Roetzel, W. (2000). Conceptions for heat transfer correlation of nanofluids. *Int. J. of Heat and Mass Transf.*, Vol. 43, No. 19, pp. 3701–3707.

2. Masuda, H., Ebata, A., Teramae, K. and Hishinuma, N. (1993). Alteration of thermal conductivity and viscosity of liquid by dispersing ultra-fine particles. *Netsu Bussei*, Vol. 7, pp. 227–233.

3. Choi, S. U. S. (1995). Enhancing thermal conductivity of fluids with nanoparticles, in: D.A. Siginer, H.P. Wang (Eds.), Developments and applications of non-newtonian flows. *FED*, Vol. 231/MD–Vol. 66, ASME, New York, pp. 99–105.

4. Khanafer, K., Vafai, K. & Lightstone, M. (2003). Buoyancy-driven heat transfer enhancement in a two-dimensional enclosure utilizing nanofluids. *Int. J. of Heat and Mass Transf.*, Vol. 46, No. 19, pp. 3639–3653.

5. Ranjbar, A. A., Kashani, S., Hosseinizadeh, S. F. & Ghanbarpour, M. (2011). Numerical heat transfer studies of a latent heat storage system containing nano-enhanced phase change material. *Therm. Sci.*, Vol. 15, No. 1, pp. 169-181.

6. Sebti, S. S., Khalilarya, S. H., Mirzaee, I., Hosseinizadeh, S. F., Kashani, S. & Abdollahzadeh, M. (2011). A numerical investigation of solidification in horizontal concentric annuli filled with nano-enhanced phase change material (NEPCM). *World Appl. Sci. J.*, Vol. 13, No. 1, pp. 09-15, 2011.

7. Benzi, R., Succi, S. & Vergassola, M. (1992). The lattice Boltzmann equation: Theory and applications. *Phys. Rep.*, Vol. 222, No. 3, pp. 145-197.

8. Chen, S. & Doolen, G. D. (1998). Lattice Boltzmann method for fluid flows. *Annu. Rev. Fluid Mech.*, Vol. 30, pp. 329-364.

9. Semma, E., Ganaoui, M. El. & Bennacer, R. (2007). Lattice Boltzmann method for melting/solidification problems. *Comptes Rendus Mécanique*, Vol. 335, No. 5-6, pp. pp. 295-303.

10. Semma, E., Ganaoui, M. El., Bennacer, R. & Mohamad, A. A. (2008). Investigation of flows in solidification by using the lattice Boltzmann method. *Int. J. Therm. Sci.*, Vol. 47, No. 3, pp. 201-208.

11. Rabienataj Darzi, A. A., Farhadi, M., Sedighi, K., Fattahi, E. & Nemati, H. (2011). Mixed convection simulation of inclined lid driven cavity using lattice Boltzmann method. *Iranian Journal of Science & Technology, Transections of Mechanical Engineering*, Vol. 35, No. M1, pp. 209-219.

12. Xuan, Y. & Yao, Z. (2005). Lattice Boltzmann model for nanofluids. *Heat Mass Transf.*, Vol. 41, No. 3., pp. 199-205.

13. Xuan, Y., Yu, K. & Li, Q. (2005). Investigation on flow and heat transfer of nanofluids by the thermal Lattice Boltzmann model. *Prog. Comput. Fluid Dyn.*, Vol., Vol. 5, No. 1-2, pp. 13-19.

14. Jourabian, M., Farhadi, M., Sedighi, K., Rabienataj Darzi, A. A. & Vazifeshenas, Y., Simulation of natural convection melting in a cavity with fin using lattice Boltzmann method. *Int. J. Numer. Meth. Fluids*, Vol. 70, No 3, pp. 313-325.

15. Nemati, H., Farhadi, M., Sedighi, K. & Darzi, A. A. R. (2010). Lattice Boltzmann simulation of nanofluid in lid-driven cavity. *Int. Commun. Heat Mass Transf.*, Vol. 37, No. 10., pp. 1528-1534.

16. Kao, P. H. & Yang, R. J. (2007). Simulating oscillatory flows in Rayleigh–Benard convection using the lattice Boltzmann method. *Int. J. of Heat and Mass Transf.*, Vol. 50, No. 17-18, pp. 3315–3328.

17. Peng, Y., Shu, C. & Chew, Y. T. (2003). Simplified thermal lattice Boltzmann model for incompressible thermal flows. *Phys. Rev. E*, Vol. 68, No. 2, pp. 1-8.

18. Barrios, G., Rechtman, R., Rojas, J. & Tovar, R. (2005). The lattice Boltzmann equation for natural convection in a two-dimensional cavity with a partially heated wall. *J. Fluid Mech.*, Vol. 522, pp. 91–100.

19. Yang, Y. T. & Lai, F. H. (2011). Numerical study of flow and heat transfer characteristics of alumina-water in a microchannel using lattice Boltzmann method. *Int. Commun. Heat Mass Transf.*, Vol. 38, No. 5, pp. 607-614.

20. Lai, F. H. & Yang, Y. T. (2011). Lattice Boltzmann simulation of natural convection heat transfer of Al_2O_3/water nanofluids in a square enclosure. *Int. J. of Therm. Sci.*, Vol. 50, No. 10, pp. 1930-1941.

21. He, Y., Qi, C., Hu, Y., Qin, B., Li, F. & Ding, Y. (2011). Lattice Boltzmann simulation of alumina-water nanofluid in a square cavity. *Nanoscale Res. Lett.*, Vol. 6, No. 1, p. 184.

22. Kefayati, G. H. R., Hosseinizadeh, S. F., Gorji, M. & Sajjadi, H. (Lattice Boltzmann simulation of natural convection in tall enclosure using water/SiO_2 nanofluid, Int. Commun. Heat Mass Transf., Vol. 38, No. 6, pp. 798-805.

23. Bertrand, O., Binet, B., Combeau, H., Couturier, S., Delannoy, Y., Gobin, D., Lacroix, M., Quere, P. L., Medale, M., Mencinger, J., Sadat, H. & Vieira, G. (1999). Melting driven by natural convection A comparison exercise: first results. *Int. J. of Therm. Sci.*, Vol. 38, 1, pp. 5-26.

24. Tan, L. & Zabaras, N. (2006). A level set simulation of dendritic solidification with combine features of front-tracking and fixed-domain methods. *J. of Comput. Phys.*, Vol. 211, No. 1, pp. 36-63.

25. Jin, C. & Xu, K. (2006). An adaptive grid method for two-dimensional viscous flows. *J. of Comput. Phys.*, Vol. 218, No. 1, pp. 68-81.

26. Boettinger, W. J., Warren, J. A., Beckermann, C. & Karma, A. (2002). Phase-field simulation of solidification. *Annu. Rev. of Mater. Res.*, Vol. 32, pp. 163-194.

27. Benard, C., Gobin, D. & Martinez, F. (1985). Melting in rectangular enclosures: experiments and numerical simulations. *J. of Heat Transf.*, Vol. 107, No. 4, pp. 794-803.

28. Wolff, F. & Viskanta, R. (1987). Melting of pure metal from a vertical wall. *Exp. Heat Transf.*, Vol. 1, No. 1, pp. 17-30.

29. Wang, Y., Amiri, A. & Vafai, K. (1999). An experimental investigation of the melting process in a rectangular enclosure. *Int. J. of Heat and Mass Transf.*, Vol. 42, No. 19, pp. 3659-3672.

30. Jany, P. & Bejan, A. (1988). Scaling theory of melting with natural convection in an enclosure. *Int. J. of Heat and Mass Transf.*, Vol. 31, No. 6, pp. 1221-1235.

31. Zhang, Z. & Bejan, A. (1989). The problem of time-dependent natural convection melting with conduction in the solid. *Int. J. of Heat and Mass Transf.*, Vol. 32, No. 12, pp. 2447-2457.

32. Usmani, A. S., Lewis, R. W. & Seetharamu, K. N. (1992). Finite element modelling of natural-convection-controlled change of phase. *Int. J. Numer. Meth. Fluids*, Vol. 14, No. 9, pp. 1019-1036.

33. Chatterjee, D. & Chakraborty, S. (2005). An enthalpy-based lattice Boltzmann model for diffusion dominated solid-liquid phase transformation. *Phys. Lett. A*, Vol. 341, No. 1-4, pp. 320-330.

34. Javierre, E., Vuik, C., Vermolen, F. J. & van der Zwaag, S. (2006). A comparison of numerical models for one-dimensional Stefan problems. *J. Comput. Appl. Math.*, Vol. 192, No. 2, pp. 445-459.

35. Khodadadi, J. M. & Hosseinizadeh, S. F. (2007). Nanoparticle-enhanced phase change materials (NEPCM) with great potential for improved thermal energy storage. *Int. Commun. Heat Mass Transf.*, Vol. 34, No. 5, pp. 534–543.

36. Jiaung, W. S., Ho, J. R. & Kuo, C. P. (2001). Lattice-Boltzmann method for the heat conduction problem with phase change. *Nume. Heat Transf. Part B*, Vol. 39, No. 6, pp. 167-187.

37. Miller, W. & Succi, S. (2002). A lattice Boltzmann model for anisotropic crystal growth from melt. *J. Stat. Phys.*, Vol. 107, No. 1-2, pp. 173-186.

38. Rasin, I., Miller, W. & Succi, S. (2005). Phase-field lattice kinetic scheme for the numerical simulation of dendritic growth. *Phys. Rev. E*, Vol. 72, No. 6, pp. 1-10.

39. Medvedev, D. & Kassner, K. (2005). Lattice Boltzmann scheme for crystal growth in external flows. *Phys. Rev. E*, Vol. 72, No. 6, pp. 1-10.

40. Huber, C., Parmigiani, A., Chopard, B., Manga, M. & Bachmann, O. (2008). Lattice Boltzmann model for melting with natural convection. *Int. J. Heat Fluid Flow*, Vol. 29, No. 5, pp. 1469-1480.

41. Patel, H. E., Pradeep, T., Sundararajan, T., Dasgupta, A., Dasgupta, N. & Das, S. K. (2005). A micro convection model for thermal conductivity of nanofluid. *PRAMANA-J. Phys.*, Vol. 65, No. 5 pp. 863–869.

42. Succi, S. (2001). *Lattice Boltzmann equation for fluid dynamics and beyond.* Clarendon Press, Oxford.

43. He, X., Chen, S. & Doolen, G. D. (1998). A novel thermal model for the lattice Boltzmann method incompressible limit. *J. of Comput. Phys.*, Vol. 146, No. 6, pp. 282-300.

44. Hou, S., Zou, Q., Chen, S., Doolen, G. & Cogley, A. C. (1995). Simulation of cavity flow by the lattice Boltzmann method. *J. of Comput. Phys.*, Vol. 118, No. 2, pp. 329-347.

45. Shan, X. (1997). Simulation of Rayleigh-Benard convection using a lattice Boltzmann method. *Phys. Rev. E*, Vol. 55, No. 2, pp. 2780-2788.

46. Guo, Z., Shi, B. & Zheng, C. (2002). A coupled lattice BGK model for the Boussinesq equations. *Int. J. Numer. Meth. Fluids*, Vol. 39, No. 4, pp. 325-342.

47. Das, R., Mishra, S. C. & Uppaluri, R. (2009). Retrieval of thermal properties in a transient conduction–radiation problem with variable thermal conductivity. *Int. J. of Heat and Mass Transf.*, Vol. 52, No. 11-12, pp. 2749–2758.

48. Wang, M., Wang, J., Pan, N. & Chen, S. H. (2007). Mesoscopic predictions of the effective thermal conductivity for micro scale random porous media. *Phys. Rev. E*, Vol. 75, No. 3, pp. 1-10.

49. Vahl Davis, G. D. (1983). Natural convection of air in a square cavity: a benchmark numerical solution. *Int. J. Numer. Meth. Fluids*, Vol. 3, No. 4, pp. 249-264.